Bulk and Surface Modes in a 1D Gyro-Uniaxial Photonic Crystal

Daniele B. Provenzano* and Giuseppe C. la Rocca†
Scuola Normale Superiore, I-56126 Pisa, Italy
(Dated: December 11, 2024)

We examine the features of electromagnetic bulk and surface modes in a 1D Photonic Crystal made up of lossless gyroelectric and uniaxial layers. We find a configuration that supports the propagation of a new type of surface mode which can have either positive or negative group velocity, depending on the signs of the uniaxial permittivities. We also show how introducing gyrotropy alters certain bulk bands and eliminates others. Exploiting an Otto configuration, we provide the analysis of a finite system where near-zero reflectivity values correspond to large Goos–Hänchen Shifts. We also explore low-symmetry configurations where waves exhibit non-reciprocal behaviors.

I. INTRODUCTION

In the field of modern photonics, the intricate interplay between light and matter has opened the way for groundbreaking discoveries and technological advancements. In the last few decades, considerable attention has been focused on the properties of Photonic Crystals (PhCs) [1, 2], which is primarily due to their application in controlling the flow of light.

The optical properties of PhCs are profoundly influenced by the characteristics of the media they are made of. In isotropic materials, both wave polarization and refractive index do not depend on the direction of wave propagation. Conversely, in anisotropic materials such quantities may depend on the propagation direction. Such low symmetry configurations lead to odd electromagnetic phenomena, such as Faraday rotation in gyrotropic media [3, 4]. Consequently, PhCs crafted from anisotropic materials exhibit markedly different characteristics compared to their isotropic counterparts. Notably, anisotropic PhCs represent a rich resource due to their controllable dispersion, offering avenues for the creation of tunable optical devices [5–8]. By harnessing external electric or magnetic fields, such as those facilitated by liquid crystals, it becomes feasible to manipulate and adjust the properties of these PhCs, including the opening, closing, or shifting of band gaps [9].

Beyond bulk modes, PhCs harbor the potential to support the propagation of Electromagnetic Surface Waves (ESWs). Such waves have garnered attention since Jonathan Zenneck's work in 1907 [10]. These modes travel along interfaces separating two media while remaining localized in the transverse direction. Among the most notable examples of ESWs are Surface Plasmon-Polaritons (SPPs), characterized by a Transverse Magnetic (TM) nature, capable of propagating at the interface between two isotropic media with permittivities of opposite signs [11]. As for interfaces involving gyrotropic media, ESWs show non reciprocal features such as the asymmetry between forward and backward propagations [12–14]. In the context of periodic structures, prominent types of ESWs include Tamm Waves and Bloch Surface Waves [15–24].

In this work, we characterize bulk and surface waves that can propagate in a one-dimensional PhC composed of lossless gyroelectric and uniaxial layers. While previous works have described light propagation in such two media separately [23, 25], their combination has never been analyzed before.

Our investigation reveals that, when the uniaxial components behave as Hyperbolic Materials (HMs), a new kind of ESWs can propagate through the structure. Such modes exhibit either forward or backward propagation features, i.e. positive or negative group velocity, depending on the specific type of HM involved. This feature is pivotal for developing new photonic devices with controllable propagation directions for light. Moreover, we show that such waves have a much greater penetration depth into the bulk compared to Tamm waves and SPPs. It is well established that photonic crystals act as frequency filters, typically relying on bulk modes for this purpose. In our case, the significantly different penetration depths of SWs would allow the control of signal transmission through surface modes rather than bulk modes.

We also show that the introduction of gyrotropy into the system significantly deformes the photonic bands. This suggests that the electromagnetic response of the realistic system could be tuned just by varying the value of the external magnetic field. In this way, one can freely modify the allowed frequency ranges within the structure.

We subsequently conduct a brief analysis of a finite system, composed of a few periods, where such effects can be found by looking at the reflection spectra using an Otto configuration. In this configuration, we show that near-zero values of the reflection coefficient correspond to non-trivial values of the Goos–Hänchen Shift (GHS). Since the GHS is related to the excitation of SWs, it can be either positive or negative depending on the sign of the group velocity characterizing the relative surface

* daniele.provenzano@sns.it
† Also at NEST, Piazza S. Silvestro, 12, I-56127 Pisa PI.

mode. Finally, we propose lower-symmetry configurations whose reflectivity is not symmetrical with respect to the inversion of the incidence angle, highlighting their non-reciprocal features due to gyrotropy.

II. ANISOTROPIC MULTILAYERED STRUCTURES

Let us consider a multilayered system consisting of an ordered succession of two lossless material slabs, whose thicknesses and dielectric tensors are, respectively, $d_1, \boldsymbol{\epsilon}_1$ and $d_2, \boldsymbol{\epsilon}_2$, as depicted in fig. 1(a). Let the spatial periodicity of the stratified medium be $L = d_1 + d_2$ and $\hat{z}$ be the growth direction, such that the overall dielectric function on the structure can be written as follows

$$\boldsymbol{\epsilon} = \begin{cases} \boldsymbol{\epsilon}_1 & mL < z < mL + d_1, \\ \boldsymbol{\epsilon}_2 & mL + d_1 < z < (m+1)L, \end{cases}$$

where m is an integer number. We consider a multilayered structure composed of gyroelectric and uniaxial layers, such that their dielectric tensors read

$$\boldsymbol{\epsilon}_1 = \epsilon_0 \begin{pmatrix} \epsilon_g & 0 & 0 \\ 0 & \epsilon_g & ig \\ 0 & -ig & \epsilon_g \end{pmatrix}, \quad \boldsymbol{\epsilon}_2' = \epsilon_0 \begin{pmatrix} \epsilon_\perp & 0 & 0 \\ 0 & \epsilon_\parallel & 0 \\ 0 & 0 & \epsilon_\perp \end{pmatrix}, \quad (1)$$

in their respective principal coordinate systems. As for the uniaxial medium, let us initially consider the general configuration wherein its optical axis is neither parallel nor perpendicular to the interface between the two media. Hence, we have to rotate its dielectric tensor by means of the rotation matrix

$$\boldsymbol{R}_x(\alpha) = \begin{pmatrix} 1 & 0 & 0 \\ 0 & \cos\alpha & \sin\alpha \\ 0 & -\sin\alpha & \cos\alpha \end{pmatrix}.$$

In our coordinate system, the uniaxial dielectric tensor reads

$$\boldsymbol{\epsilon}_2 = \boldsymbol{R}_x(\alpha)\ \boldsymbol{\epsilon}_u'\ \boldsymbol{R}_x(-\alpha) = \epsilon_0 \begin{pmatrix} \epsilon_{xx} & 0 & 0 \\ 0 & \epsilon_{yy} & \epsilon_{yz} \\ 0 & \epsilon_{zy} & \epsilon_{zz} \end{pmatrix},$$

where the matrix elements are

$$\begin{aligned} \epsilon_{xx} &= \epsilon_\perp, \\ \epsilon_{yy} &= \epsilon_\perp \sin^2\alpha + \epsilon_\parallel \cos^2\alpha, \\ \epsilon_{yz} &= \epsilon_{zy} = \left(\epsilon_\perp - \epsilon_\parallel\right) \sin\alpha \cos\alpha, \\ \epsilon_{zz} &= \epsilon_\perp \cos^2\alpha + \epsilon_\parallel \sin^2\alpha. \end{aligned}$$

For analytical convenience, we focus on anisotropic configurations where TE and TM modes can be decoupled, while low-symmetry configurations will be numerically investigated in section V. Non-trivial results will concern only the TM-polarization, thus it is appropriate to consider the following form for the magnetic field, accounting for both forward and backward modes:

$$H_x^m(y,z) = \begin{cases} \left[a_m e^{ik_u(z-mL)} + b_m e^{-ik_u(z-mL)}\right] e^{i(k_y y - \omega t)} & mL < z < mL + d_u, \\ \left[c_m e^{ik_g(z-mL)} + d_m e^{-ik_g(z-mL)}\right] e^{i(k_y y - \omega t)} & mL + d_u < z < (m+1)L, \end{cases} \quad (2)$$

where u stands for *uniaxial* and g for *gyrotropic*, k_u and k_g represent the z-components of the wave vectors, whereas $L \equiv d_u + d_g$, d_u and d_g are, respectively, the period of the structure and the thicknesses of the two slabs. The coefficients a_m, b_m, c_m, d_m are the amplitudes of forward and backward modes relative to each medium, as outlined in fig. 1(b).

Applying the continuity conditions for H_x and E_y on the two boundaries marked by red arrows in fig. 1(b), leads to a four-equations system relating the six variables a_m, b_m, c_m, d_m, c_{m-1} and d_{m-1}. As shown in appendix A, the whole algebraic system can be recast in order to express c_{m-1} and d_{m-1} as functions of c_m and d_m:

$$\begin{pmatrix} c_{m-1} \\ d_{m-1} \end{pmatrix} = \begin{pmatrix} A & B \\ C & D \end{pmatrix} \begin{pmatrix} c_m \\ d_m \end{pmatrix}. \quad (3)$$

where A, B, C and D are complex coefficients which will be derived in the next section. We will use this formalism in order to find the eigenmodes in a one dimensional periodic structure.

III. ANISOTROPIC PHOTONIC CRYSTALS

If we let the number of layers become infinite, what we obtain is a Photonic Crystal. In such a periodic system, the Bloch theorem assures that the solution to the Helmholtz equation is a Bloch wave, namely a wave function which can be written as the product of a plane wave and a periodic term

$$\mathbf{H}(z) = \mathbf{H}_B(z)\ e^{iK_B z}, \quad (4)$$

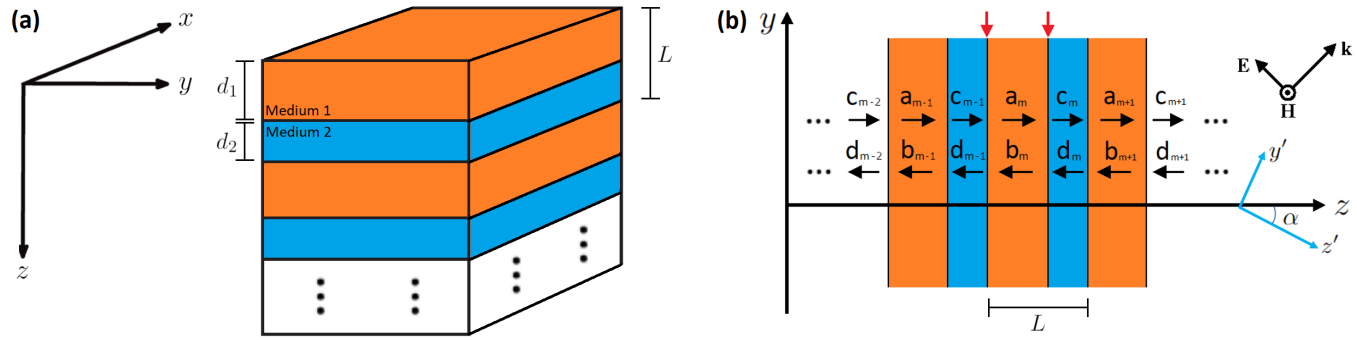

FIG. 1. (a) Outline of the 1D-periodic multilayer structure. (b) Outline of the yz plane section of the periodic structure under consideration. Here, y' and z' represent the principal axes of the hyperbolic slabs.

where $\mathbf{H}_B(z) = \mathbf{H}_B(z+L)$ is a periodic function and K_B is the Bloch wave number [26]. Following the procedure shown in [27], we must solve the following eigenvalue problem

$$\begin{pmatrix} A & B \\ C & D \end{pmatrix} \begin{pmatrix} c_m \\ d_m \end{pmatrix} = e^{-iK_B L} \begin{pmatrix} c_m \\ d_m \end{pmatrix}, \tag{5}$$

whose solutions are

$$\begin{pmatrix} c_m \\ d_m \end{pmatrix} = \begin{pmatrix} B \\ e^{-iK_B L} - A \end{pmatrix}, \tag{6}$$

where

$$K_B = \pm \frac{1}{L} \cos^{-1}\left(\frac{A+D}{2}\right). \tag{7}$$

As pointed out in appendix A, the eigenvalues are one the reciprocal of each other because the matrix in eq. (5) is unitary. If K_B is a real number, the eigenvalues represent propagating waves, whereas complex values of K_B correspond to damped waves in the bulk. Due to the properties of the cosine function, we can distinguish two scenarios: if $A + D \in \mathbb{R}$ and $A + D < 2$, the Bloch wave can propagate trough the PhC, otherwise it will decay inside the bulk [26, 27]. The latter situation corresponds to the band gap.

We can derive the coefficients A, B, C, D in the TM case by means of eqs. (A1)-(A4). They turn out to be

$$A_{TM} = e^{ik_u d_u}\left\{\cos k_g d_g + \frac{i}{2}\sin k_g d_g \left[\frac{\epsilon_\parallel \epsilon_\perp k_g}{\epsilon_v \epsilon_{zz} k_u} + \frac{\epsilon_v \epsilon_{zz} k_u}{\epsilon_\parallel \epsilon_\perp k_g} - \frac{\epsilon_\parallel \epsilon_\perp}{\epsilon_v \epsilon_{zz}} \frac{k_y^2}{k_u k_g} Z^2\right]\right\}, \tag{8}$$

$$B_{TM} = \frac{i}{2} e^{-ik_u d_u} \sin k_g d_g \left\{\frac{\epsilon_\parallel \epsilon_\perp k_g}{\epsilon_v \epsilon_{zz} k_u} - \frac{\epsilon_v \epsilon_{zz} k_u}{\epsilon_\parallel \epsilon_\perp k_g} - \frac{\epsilon_\parallel \epsilon_\perp}{\epsilon_v \epsilon_{zz}} \frac{k_y^2}{k_u k_g} Z^2 + 2Z\frac{k_y}{k_g}\right\}, \tag{9}$$

$$C_{TM} = -\frac{i}{2} e^{ik_u d_u} \sin k_g d_g \left\{\frac{\epsilon_\parallel \epsilon_\perp k_g}{\epsilon_v \epsilon_{zz} k_u} - \frac{\epsilon_v \epsilon_{zz} k_u}{\epsilon_\parallel \epsilon_\perp k_g} - \frac{\epsilon_\parallel \epsilon_\perp}{\epsilon_v \epsilon_{zz}} \frac{k_y^2}{k_u k_g} Z^2 - 2Z\frac{k_y}{k_g}\right\}, \tag{10}$$

$$D_{TM} = e^{-ik_u d_u}\left\{\cos k_g d_g - \frac{i}{2}\sin k_g d_g \left[\frac{\epsilon_\parallel \epsilon_\perp k_g}{\epsilon_v \epsilon_{zz} k_u} + \frac{\epsilon_v \epsilon_{zz} k_u}{\epsilon_\parallel \epsilon_\perp k_g} - \frac{\epsilon_\parallel \epsilon_\perp}{\epsilon_v \epsilon_{zz}} \frac{k_y^2}{k_u k_g} Z^2\right]\right\}, \tag{11}$$

where we defined

$$\epsilon_v \equiv \frac{\epsilon_g^2 - g^2}{\epsilon_g},$$

$$Z \equiv \frac{\epsilon_{yz}\epsilon_v}{\epsilon_\parallel \epsilon_\perp} - i\frac{g}{\epsilon_g}, \tag{12}$$

Notice that Z reduces to zero if both media are isotropic and, consequently, the matrix elements (8)-(11) reduce

to the expressions commonly documented in literature [1, 26, 27]. Furthermore, eq. (7) becomes

$$K_{TM}^{B} = \frac{1}{L}\cos^{-1}\left(\cos k_g d_g \cos k_u d_u - \mathcal{F}\sin k_g d_g \sin k_u d_u\right), \tag{13}$$

where we defined

$$2\mathcal{F} \equiv \frac{\epsilon_{\parallel}\epsilon_{\perp}k_g}{\epsilon_v \epsilon_{zz} k_u} + \frac{\epsilon_v \epsilon_{zz} k_u}{\epsilon_{\parallel}\epsilon_{\perp}k_g} - \frac{\epsilon_{\parallel}\epsilon_{\perp}}{\epsilon_v \epsilon_{zz}}\frac{k_y^2}{k_u k_g} Z^2. \tag{14}$$

As mentioned in the previous section, we only focus on the TM polarization because TE modes obey the very same equations of the isotropic case.

Before moving on, it is essential to make a significant observation. As evident from eqs. (13) and (14), the presence of Z ensures that K_B has an imaginary part if $g \neq 0$ and $\epsilon_{yz} \neq 0$ simultaneously, for any real values of ω and k_y. This is surprising, especially considering that it holds true even for lossless structures, such as the ones we aim to analyze. In any case, the band diagram is almost empty because, apart from normal incidence and a few other cases, no mode can propagate into the bulk. This last statement will be further examined during the discussion of the numerical results.

We aim to investigate non-trivial scenarios involving gyrotropy, hence we are compelled to restrict our analysis to the case $\alpha = k\pi/2$, where $k \in \mathbb{Z}$.

In the upcoming section, we will employ eq. (13) to derive band diagrams for TM modes within our anisotropic PhC. Our objective is to identify surface states within the band gaps, where bulk modes are not allowed to propagate.

IV. MODES IN A SEMI-INFINITE PHOTONIC CRYSTAL

Valuable insights can be gathered by exploring the surface modes permitted to propagate in PhCs [17, 28], as we will demonstrate below.

When a PhC is cut along one interface between two consecutive slabs, two semi-infinite PhCs are created. The dispersion relation for surface waves propagating on a semi-infinite PhC bordering a dielectric half space is [22, 29]

$$e^{iK_B L} - A - \frac{Bc}{\omega\epsilon_I}\sqrt{\epsilon_I\left(\frac{\omega}{c}\right)^2 - k_y^2} = 0, \tag{15}$$

where ϵ_I is the dielectric constant of the isotropic dielectric half space. Eq. (15) enables us to identify and graphically represent the surface modes directly on the reduced band diagrams that characterize the system.

Prior to presenting our numerical findings, it's important to introduce the frequency dependence of the dielectric functions. We choose to consider the following dispersion for the uniaxial medium permittivities

$$\epsilon_{\perp,\parallel} = \epsilon_{\infty}\left(1 - \frac{\omega_{p_{\perp,\parallel}}^2}{\omega^2}\right). \tag{16}$$

Such response functions with anisotropic plasma frequencies characterize the behavior of media that exist in nature [30, 31] or can be artificially engineered using multilayer or nanowire array geometries [32–34]. In such engineered media, non-local effects may play a significant role in shaping the dispersion of EWs, as discussed in [35, 36]. We neglect such effects in the present work.

As ω varies, (16) may describe an anisotropic metal ($\omega < \min(\omega_{p_\perp}, \omega_{p_\parallel})$), an anisotropic dielectric ($\omega > \max(\omega_{p_\perp}, \omega_{p_\parallel})$) or a hyperbolic medium ($\min(\omega_{p_\perp}, \omega_{p_\parallel}) < \omega < \max(\omega_{p_\perp}, \omega_{p_\parallel})$). The last regime is of particular interest when it comes to surface modes, as shown in fig. 2. Its rows correspond to the three different scenarios $\omega_{p,\parallel} = \omega_{p,\perp}$, $\omega_{p,\parallel} < \omega_{p,\perp}$ and $\omega_{p,\parallel} > \omega_{p,\perp}$, respectively. Instead, columns correspond to non-gyrotropy (left) and gyroelectric (right) cases. It should be specified that the surface modes in fig. 2 only concern the configuration where the semi-infinite crystal terminates with a gyrotropic slab. If this were not the case, the dispersion of the surface waves would be slightly different, but all their characteristic features would remain the same.

- Fig. 2(a)-(b), $\omega_{p,\parallel} = \omega_{p,\perp} \equiv \omega_p$. Two distinct types of surface waves are observed: a truncated SPP below the threshold $\omega = \omega_p$, and Tamm waves in the domain $\omega > \omega_p$, where the metallic constituents demonstrate dielectric behavior ($\epsilon_\parallel, \epsilon_\perp > 0$).
  When gyrotropy is switched on within the dielectric layers, the lower bands get modified such that the SPP no longer exists. Conversely, Tamm waves experience subtle modifications but do not undergo significant alterations.

- Fig. 2(c)-(d), $\omega_{p,\parallel} < \omega_{p,\perp}$. The horizontal bulk plasmon line undergoes a significant division into numerous bulk bands, situated within the range delineated by the plasma frequencies $\omega_{p,\parallel}$ and $\omega_{p,\perp}$, where the anisotropic metallic components behave as Type 2 HMMs [37, 38]. Notably, an intermediate surface mode emerges within each band gap separating the bulk bands. These waves have a positive group velocity, thus they propagate in the forward direction.
  Interestingly, the introduction of gyrotropy has minimal impact on surface modes, despite some degenerate bands undergoing division. For enhanced clarity, fig. 3(a) illustrates two transversal sections of the reduced band diagram.

- Fig. 2(e)-(f), $\omega_{p,\parallel} > \omega_{p,\perp}$. Similar to the previous scenario, an infinite array of bulk bands oc-

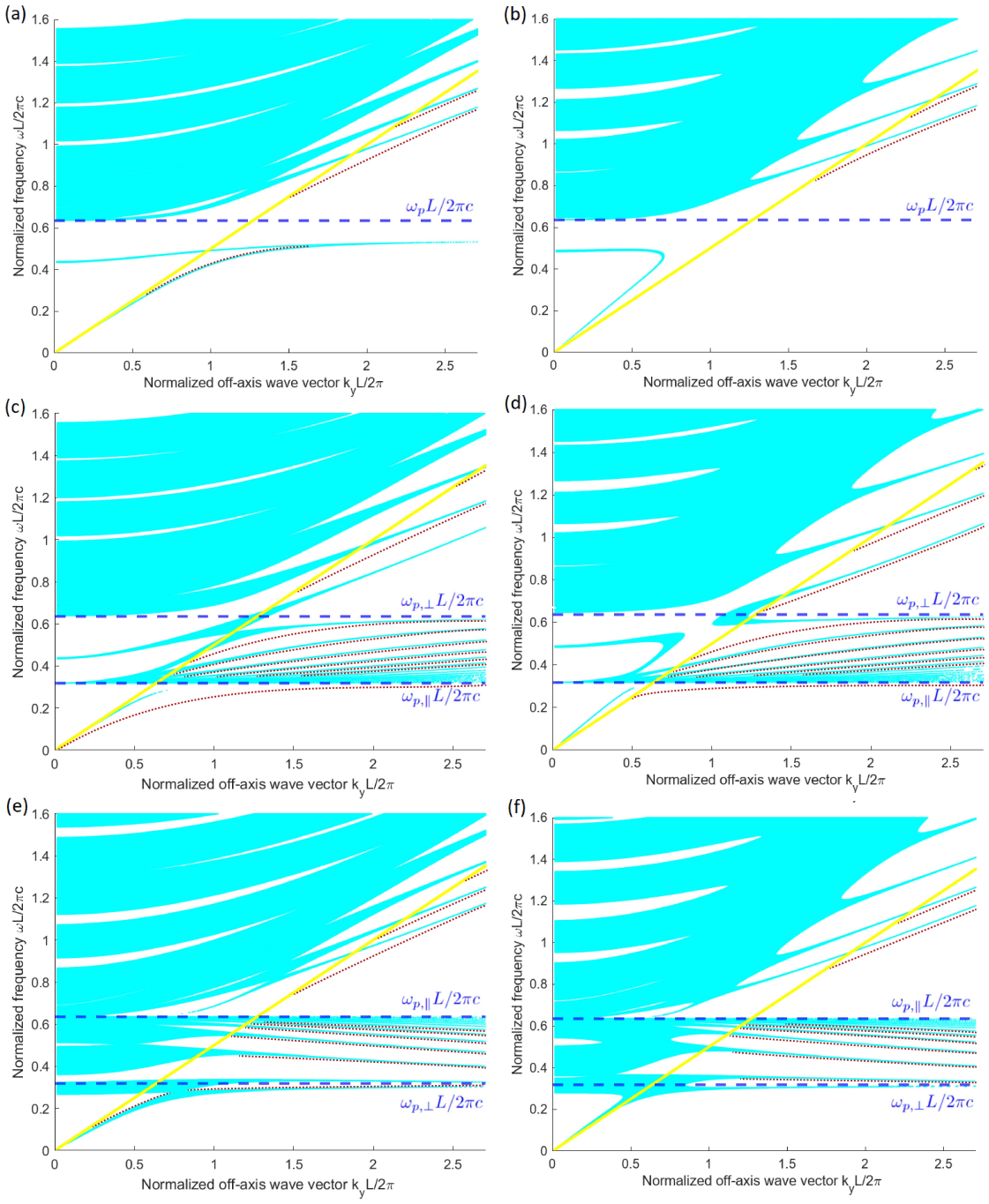

FIG. 2. Reduced band diagrams for TM waves in a metal-dielectric PhC, for different values of the structural parameters. The red dotted lines correspond to surface modes, whereas the yellow line represents the light line of the dielectric half-space. The considered structural parameters are $\epsilon_I = 4$, $\epsilon_g = 3$, $\epsilon_\infty = 8$, $d_g = 0.56\ \mu m$, $d_u = 0.44\ \mu m$ and $\alpha = \pi/2$. (a) $\omega_{p,\parallel} = \omega_{p,\perp}$, $g = 0$, (b) $\omega_{p,\parallel} = \omega_{p,\perp}$, $g = 1.5$, (c) $\omega_{p,\parallel} < \omega_{p,\perp}$, $g = 0$, (d) $\omega_{p,\parallel} < \omega_{p,\perp}$, $g = 1.5$, (e) $\omega_{p,\parallel} > \omega_{p,\perp}$, $g = 0$, (f) $\omega_{p,\parallel} > \omega_{p,\perp}$, $g = 1.5$.

cupies the domain delineated by the plasma frequencies $\omega_{p,\perp}$ and $\omega_{p,\parallel}$. Within this domain, the anisotropic metallic components behave as Type 1 HMMs [37, 38]. Notably, all the intermediate surface waves demonstrate a negative group velocity, implying their propagation in the backward direction. Furthermore, the SPP undergoes bifurcation into two branches due to the convergence of lower bands.

When gyrotropy is switched on, the lower bands get modified such that the SPP no longer exists. For enhanced clarity, fig. 3(b) illustrates two transver-

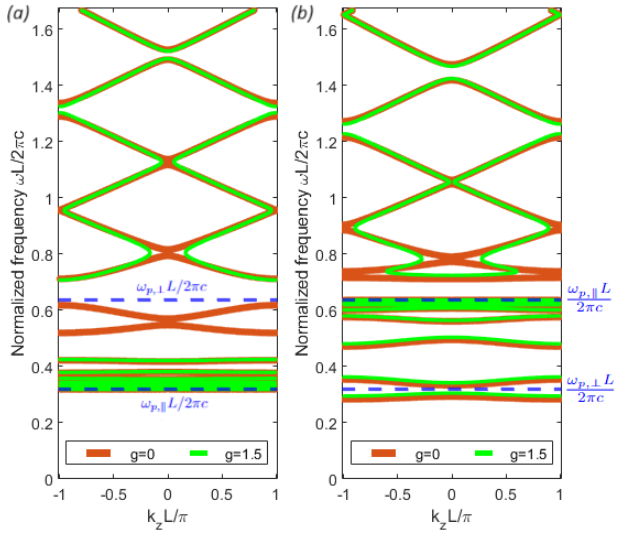

FIG. 3. Transversal sections of the reduced band diagram shown in fig. 2, for $k_y L/2\pi = 1$. Panel (a) corresponds to fig. 2(c)-(d), whereas panel (b) corresponds to fig. 2(e)-(f). As gyrotropy is switched on, a large number of bulk bands appear slightly above or below the $\omega_{p,\parallel} L/2\pi c$ line.

sal sections of the reduced band diagram.

In summary, these intermediate waves [39] can propagate either forward or backward, depending on the hyperbolic behavior of the uniaxial material constituting the structure. Similar results were found in [40] for the non-gyrotropic case. In such work, the intermediate surface modes are referred to as *Tamm-Langmuir surface waves*.

As previously stated, the presence of gyrotropy in the system modifies some bulk bands, as can be clearly seen in fig. 3. This implies that by adjusting the external magnetic field, the electromagnetic response of the system can be fine-tuned, allowing for the modification of the permissible frequency ranges within the structure.

Fig. 4 presents a comparison of the field distributions between the Tamm wave and the intermediate mode. Notably, the latter exhibits a significantly greater penetration depth than the former. It is observed that the electric field of the novel mode oscillates within the uniaxial layers without any damping. This unique feature facilitates deeper penetration of the mode into the bulk. This property may allow the control of signal transmission through surface modes rather than bulk modes.

We conclude this section by numerically investigating the observation made at the end of section III, concerning the restriction to $\alpha = k\pi/2$, where $k \in \mathbb{Z}$. As pointed out before, if $\alpha \neq k\pi/2$ then the Bloch wave number is complex almost for every non-zero value of k_y. As a further confirmation, fig. 5 shows the behavior of the imaginary part of K_B as k_y varies, for four different values of the working frequency. It is evident that $K_B \in \mathbb{C}$ almost everywhere. Notice that, depending on the working frequency, the imaginary part of K_B may be huge or approach zero at normal incidence. The first case corresponds to the band gap, where $A + D$ is now real but larger than 2. The second case corresponds to bulk propagating modes, hence this demonstrates that the band diagram is not empty at normal incidence. Moreover, apart from the case $k_y \to 0$, there may exist further values of k_y for which $\mathrm{Im}(K_B)$ becomes very small. This is due to the form of eq. (14): k_u and k_g are imaginary for high values of the off-axis wave vector, hence the imaginary part of the coefficient $\mathcal{F}$ can actually become zero for a limited number of values of k_y.

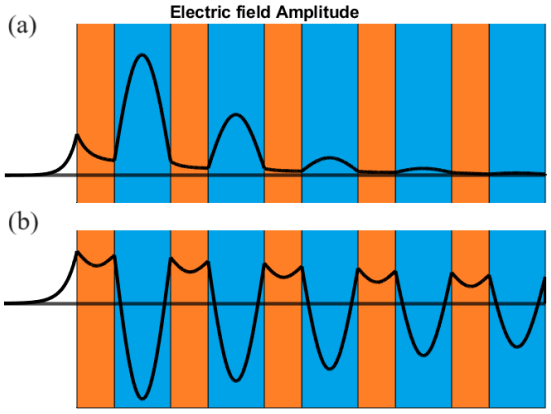

FIG. 4. Typical space distributions of the y-component of the electric field amplitude in a semi-infinite gyro-uniaxial PhC confining with vacuum. The blue regions represent the uniaxial components, whereas the orange ones represent the gyrotropic components. (a) Tamm wave. (b) Intermediate surface mode.

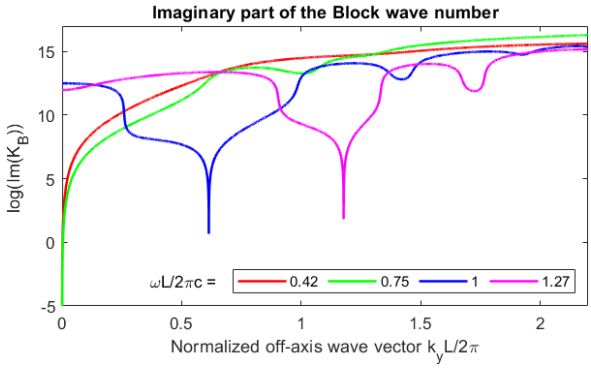

FIG. 5. Natural logarithm of the imaginary part of the Bloch wave number as a function of the off-axis wave vector, for four different values of the working frequency. The structural parameters are the same of fig. 2(d), except for $\alpha = 1$ rad.

V. FINITE MULTILAYER STRUCTURES

This final section contains a few numerical results concerning finite structures, whose properties were analyzed using the so called *Otto configuration* with a coupling prism whose refractive index is 3. As for the

numerical method, we used the 4×4 Transfer Matrix Formalism for anisotropic media, proposed by Berreman [41].

First, we conducted a brief analysis on the Goos-Hänchen Shift (GHS) [42] for finite multilayer structures. It is well-known that the GHS dramatically increases when getting close to the Brewster angle [43], at which light is totally transmitted through the system. We calculated both the reflectivity and the GHS for two structures consisting of ten periods each, in the frequency domain delimited by the two plasma frequencies $\omega_{p,\perp}$ and $\omega_{p,\parallel}$. The results are shown in fig. 6. Consistent with expectations, at angles where the reflectivity approaches zero, the GHS is positive in the case of forward modes, whereas it is negative for backward modes.

A final consideration worth making concerns bulk bands. As can be seen from eqs. (13) and (14), the dispersion of bulk bands only depends on k_y^2, hence there is no difference between positive and negative angles of incidence. Indeed, the bulk modes are not affected by non-reciprocity effects despite the presence of a gyrotropic medium. In order to break the high level of symmetry and be able to observe differences between positive and negative angles of incidence, one way is to rotate the gyroelectric components such that, in our coordinate system, their dielectric tensor reads

$$\boldsymbol{\epsilon}_1 = \epsilon_0 \begin{pmatrix} \epsilon_g & 0 & ig \\ 0 & \epsilon_g & 0 \\ -ig & 0 & \epsilon_g \end{pmatrix}. \tag{17}$$

Fig. 7 shows a comparison between the reflectivity of two multilayer structures whose gyrotropic tensors are described by eq. (1) and eq. (17). It appears evident that the latter configuration introduces asymmetry between positive and negative angles of incidence. Such configuration cannot be analyzed using the method of section III because TE and TM modes cannot be decoupled. They should be studied at the same time.

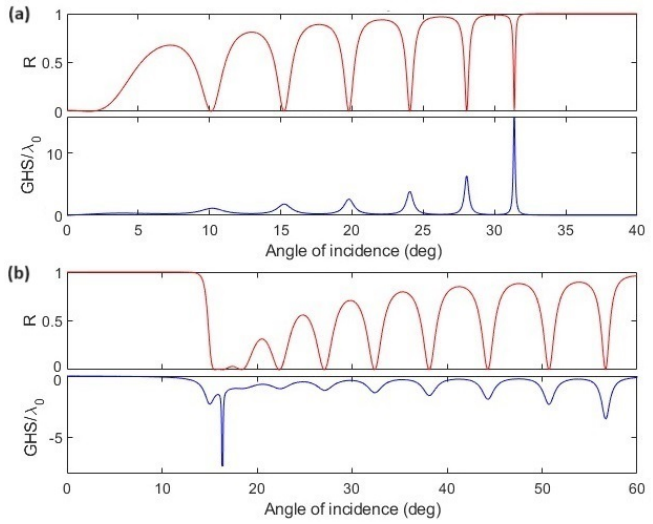

FIG. 6. Reflectivity and Goos–Hänchen Shift (in units of the incident wavelength) for two multilayer structures composed of 10 periods, calculated using the Transfer Matrix method. The structural parameters are the same as in fig. 2. (a) $\omega_{p,\parallel} < \omega_{p,\perp}$, corresponding to forward surface modes of fig. 2(d). (b) $\omega_{p,\parallel} > \omega_{p,\perp}$, corresponding to backward propagating surface modes of fig. 2(f).

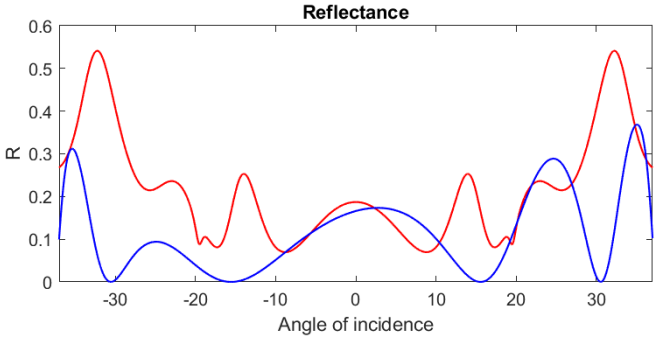

FIG. 7. Comparison between the reflectivity of gyro-uniaxial multilayer structures whose gyrotropic components are described by eq. (1) (red) and eq. (17) (blue).

VI. CONCLUSION

In conclusion, we employed an analytical method to characterize the dispersion of bulk bands and surface states in a one-dimensional PhC composed of lossless gyroelectric and uniaxial layers. This study reveals that the structure not only can support SPPs and Tamm waves, but also a new kind of ESWs. These surface waves exhibit either positive or negative group velocity, which is crucial for developing new photonic devices with controllable light propagation directions. Our analysis shows that these surface waves have a much greater penetration depth into the bulk compared to Tamm waves and SPPs. This significant difference in penetration depths allows for controlling signal transmission through surface modes rather than bulk modes, enhancing the functionality of photonic crystals as frequency filters. Furthermore, the introduction of gyrotropy into the system significantly deforms the photonic bands, indicating that the electromagnetic response can be finely tuned by varying the external magnetic field. This ability to modify the allowed frequency ranges within the structure enhances the versatility of PhCs. We also explored the reflectivity spectra of finite structures arranged in an Otto configuration. Near-zero reflectivity values correspond to high values of the Goos–Hänchen Shift (GHS), which can be either positive or negative depending on the sign of the group velocity characterizing the relative surface mode. Additionally, we examined configurations with asymmetrical reflectivity with respect to the inversion of the incidence angle, highlighting their non-reciprocal features

due to gyrotropy.

Overall, our findings underscore the potential for controlling signal transmission through novel surface modes in layered structures based on a combination of hyperbolic and gyroelectric media capitalizing on the properties of both material classes.

Appendix A: Interface Conditions

Given H_x in eq. (2), it is trivial to evaluate E_y and E_z by means of Maxwell's equations. Additionally, they imply that H_x and E_y are continuous functions along the boundaries, while E_z is not, due to the dielectric function's discontinuity. The continuity of both H_x and E_y on the boundaries on the two boundaries marked by red arrows in fig. 1(b) leads to

$$c_{m-1} + d_{m-1} = a_m e^{ik_g L} + b_m e^{-ik_g L}, \tag{A1}$$

$$c_m e^{ik_u d_u} + d_m e^{-ik_u d_u} = a_m e^{ik_g d_u} + b_m e^{-ik_g d_u}, \tag{A2}$$

$$\frac{i\epsilon_v}{\epsilon_\parallel \epsilon_\perp}\left[d_{m-1}(\epsilon_{zz}k_u + \epsilon_{zz}k_y) + c_{m-1}(\epsilon_{zz}k_y - \epsilon_{zz}k_u)\right] =$$
$$= a_m\left(ik_g - \frac{g}{\epsilon_g}k_y\right)e^{ik_g L} - b_m\left(ik_g + \frac{g}{\epsilon_g}k_y\right)e^{-ik_g L}, \tag{A3}$$

$$\frac{i\epsilon_v e^{ik_u d_u}}{\epsilon_\parallel \epsilon_\perp}\left[c_m(\epsilon_{zz}k_u + \epsilon_{yz}k_y) + d_m(\epsilon_{yz}k_y - \epsilon_{zz}k_u)e^{-2ik_u d_u}\right] =$$
$$= a_m\left(ik_g - \frac{g}{\epsilon_g}k_y\right)e^{ik_g d_u} - b_m\left(ik_g + \frac{g}{\epsilon_g}k_y\right)e^{-ik_g d_u}, \tag{A4}$$

where we defined

$$\epsilon_v \equiv \frac{\epsilon_g^2 - g^2}{\epsilon_g}.$$

The components of the wave vectors obey the following dispersion relations:

$$\epsilon_{yy}k_y^2 + \epsilon_{zz}k_u^2 + 2k_y k_u \epsilon_{yz} = \frac{\omega^2}{c^2}\epsilon_\parallel \epsilon_\perp.$$

$$k_g^2 + k_y^2 = \epsilon_v \frac{\omega^2}{c^2}.$$

Let us use a_m and b_m as free variables and recast the system (A1)-(A4) into the following form

$$\begin{pmatrix} c_{m-1} \\ d_{m-1} \end{pmatrix} = \mathbf{P}^{-1}\mathbf{Q}\begin{pmatrix} a_m \\ b_m \end{pmatrix}, \quad \begin{pmatrix} c_m \\ d_m \end{pmatrix} = \mathbf{R}^{-1}\mathbf{S}\begin{pmatrix} a_m \\ b_m \end{pmatrix},$$

where $\mathbf{P}, \mathbf{Q}, \mathbf{R}, \mathbf{S}$ are 2×2 matrices [27]. The last two equations imply

$$\begin{pmatrix} c_{m-1} \\ d_{m-1} \end{pmatrix} = \mathbf{P}^{-1}\mathbf{Q}\,\mathbf{S}^{-1}\mathbf{R}\begin{pmatrix} c_m \\ d_m \end{pmatrix}. \tag{A5}$$

The matrix

$$\mathbf{P}^{-1}\mathbf{Q}\,\mathbf{S}^{-1}\mathbf{R} \equiv \begin{pmatrix} A & B \\ C & D \end{pmatrix}$$

is unimodular because it relates the field amplitudes of equivalent layers of two consecutive cells [26, 27].

[1] J. Joannopoulos, S. Johnson, J. Winn, and R. Meade, *Photonic Crystals: Molding the Flow of Light - Second Edition* (Princeton University Press, 2011).

[2] K. Inoue and K. Ohtaka, *Photonic Crystals: Physics, Fabrication and Applications*, Vol. 94 (2004).

[3] L. D. Landau and E. M. Lifshitz, *Electrodynamics of Continuous Media* (Pergamon, 1984).

[4] A. Zangwill, *Modern Electrodynamics* (Cambridge University Press, 2012).

[5] G. Alagappan, X. Sun, P. Shum, Y. Yu, and D. Engelsen, Symmetry properties of two-dimensional anisotropic photonic crystals, Journal of the Optical Society of America. A, Optics, image science, and vision **23**, 2002 (2006).

[6] G. Alagappan, X. Sun, P. Shum, Y. Yu, and M. Doan, One-dimensional anisotropic photonic crystal with a tunable bandgap, Journal of The Optical Society of America

B-optical Physics - J OPT SOC AM B-OPT PHYSICS **23** (2006).
[7] V. Fesenko, I. Sukhoivanov, S. Shulga, and h. Shi, One-dimensional anisotropic photonic crystals based on anisotropic porous silicon (2008) pp. 457–459.
[8] K. Vytovtov and L. Mospan, One-dimensional anisotropic photonic crystal as a key element for nonreciprocal optical devices based not on the faraday effect, in *2011 41st European Microwave Conference* (2011) pp. 818–821.
[9] S. Kim and S. Kurihara, Liquid crystals for responsible photonic crystals (2018).
[10] J. Zenneck, Über die fortpflanzung ebener elektromagnetischer wellen längs einer ebenen leiterfläche und ihre beziehung zur drahtlosen telegraphie, Annalen der Physik **328**, 846 (1907).
[11] S. Maier, Plasmonics: Fundamentals and applications (2007) p. 245.
[12] R.-L. Chern and Y.-Z. Yu, Chiral surface waves on hyperbolic-gyromagnetic metamaterials, Optics Express **25**, 11801 (2017).
[13] D. B. Provenzano and G. C. la Rocca, Interface mode between gyroelectric and hyperbolic media, J. Opt. Soc. Am. B **40**, 172 (2023).
[14] Y. Zheng, J. Chen, Z. Ji, H. Lin, and Z.-Y. Li, Analytical solutions for electromagnetic surface states at the interface between metal and gyromagnetic media, J. Opt. Soc. Am. B **40**, 2815 (2023).
[15] A. Lakhtakia, T. Mackay, and C. Zhou, Electromagnetic surface waves at exceptional points, European Journal of Physics **42** (2020).
[16] J. Polo, T. Mackay, and A. Lakhtakia, Electromagnetic surface waves: A modern perspective (2013) pp. 1–293.
[17] J. Bashiri, B. Rezaei, J. Barvestani, and C. Zapata-Rodríguez, Bloch surface waves engineering in one-dimensional photonic crystals with a chiral cap layer, Journal of the Optical Society of America B **36**, 2106 (2019).
[18] T.-B. Wang, C. Yin, W.-Y. Liang, J.-W. Dong, and H.-Z. Wang, Electromagnetic surface modes in one-dimensional photonic crystals with dispersive metamaterials, JOSA B **26**, 1635 (2009).
[19] A. Akjouj, E. B. El Houssaine, L. Dobrzynski, B. Djafari-Rouhani, and G. Lévêque, Optical tamm states in semi-infinite layered photonic crystals (2021) pp. 489–527.
[20] J. Martorell, D. W. L. Sprung, and G. V. Morozov, Surface te waves on 1d photonic crystals, Journal of Optics A: Pure and Applied Optics **8**, 630 (2006).
[21] J. Barvestani, M. Kalafi, and A. Vala, Surface optical waves in semi-infinite one-dimensional photonic crystals containing alternating layers of positive and negative media with a cap layer, Acta Physica Polonica A - ACTA PHYS POL A **112** (2007).
[22] S. Feng, H.-Y. Sang, Z.-Y. Li, B.-Y. Cheng, and D.-Z. Zhang, Sensitivity of surface states to the stack sequence of one-dimensional photonic crystals, Journal of Optics A: Pure and Applied Optics **7**, 374 (2005).
[23] E. E. Narimanov, Photonic hypercrystals, Phys. Rev. X **4**, 041014 (2014).
[24] J. Pérez Huerta, P. Lopez, W. Mochán, G. Ortiz, V. Agarwal, and R. Castro-García, Reflectivity of 1d photonic crystals: A comparison of computational schemes with experimental results, International Journal of Modern Physics B **32**, 1850136 (2018).
[25] X. Zhao, Y. luo, and L. Zhou, Study on the photonic crystal made by gyrotropic medium, in *2007 International Nano-Optoelectronics Workshop* (2007) pp. 144–145.
[26] A. Yariv and P. Yeh, *Optical Waves in Crystals: Propagation and Control of Laser Radiation*, Wiley Series in Pure and Applied Optics (Wiley, 2002).
[27] P. Yeh, *Optical Waves in Layered Media*, Wiley Series in Pure and Applied Optics (Wiley, 2005).
[28] A. Vinogradov, A. Dorofeenko, A. Merzlikin, and A. Lisyansky, Surface states in photonic crystals, Physics-Uspekhi **53**, 243 (2010).
[29] T.-B. Wang, C. Yin, W.-Y. Liang, J.-W. Dong, and H.-Z. Wang, Electromagnetic surface modes in one-dimensional photonic crystals with dispersive metamaterials, JOSA B **26**, 1635 (2009).
[30] V. W. Brar, M. S. Jang, M. Sherrott, S. Kim, J. J. Lopez, L. B. Kim, M. Choi, and H. Atwater, Hybrid surface-phonon-plasmon polariton modes in graphene/monolayer h-bn heterostructures, Nano Letters **14**, 3876 (2014), pMID: 24874205.
[31] D. Grecu, Plasma frequency of the electron gas in layered structures, Phys. Rev. B **8**, 1958 (1973).
[32] O. Y. Yermakov, A. I. Ovcharenko, M. Song, A. A. Bogdanov, I. V. Iorsh, and Y. S. Kivshar, Hybrid waves localized at hyperbolic metasurfaces, Phys. Rev. B **91**, 235423 (2015).
[33] K. L. Koshelev and A. A. Bogdanov, Temperature-tunable semiconductor metamaterial, Phys. Rev. B **92**, 085305 (2015).
[34] P. A. Belov, R. Marqués, S. I. Maslovski, I. S. Nefedov, M. Silveirinha, C. R. Simovski, and S. A. Tretyakov, Strong spatial dispersion in wire media in the very large wavelength limit, Phys. Rev. B **67**, 113103 (2003).
[35] A. V. Chebykin, A. A. Orlov, A. V. Vozianova, S. I. Maslovski, Y. S. Kivshar, and P. A. Belov, Nonlocal effective medium model for multilayered metal-dielectric metamaterials, Phys. Rev. B **84**, 115438 (2011).
[36] M. A. Gorlach and P. A. Belov, Effect of spatial dispersion on the topological transition in metamaterials, Phys. Rev. B **90**, 115136 (2014).
[37] L. Ferrari, C. Wu, D. Lepage, X. Zhang, and Z. Liu, Hyperbolic metamaterials and their applications, Progress in Quantum Electronics **40** (2014).
[38] P. Shekhar, J. Atkinson, and Z. Jacob, Hyperbolic metamaterials: Fundamentals and applications, Nano Convergence **1** (2014).
[39] The word *intermediate* refers to the position of the new surface modes, which live in the frequency domain delimited by the two plasma frequencies.
[40] K. Golenitskii, K. Koshelev, and A. Bogdanov, Tamm-langmuir surface waves, Physical Review A **94** (2016).
[41] D. Berreman, Optics in stratified and anisotropic media: 4×4 matrix formulation, Journal of The Optical Society of America **62** (1972).
[42] K. Manzoor, W. Waseer, Q. Naqvi, and M. Mughal, Goos–hänchen shift observed from stratified medium, The European Physical Journal D **76** (2022).
[43] H. M. Lai and S. W. Chan, Large and negative goos–hänchen shift near the brewster dip on reflection from weakly absorbing media, Opt. Lett. **27**, 680 (2002).